IOP Publishing Superconductor Science and Technology
Supercond. Sci. Technol. 31 (2018) 035001 (8pp) https://doi.org/10.1088/1361-6668/aaa44f

Flux trapping in multi-loop SQUIDs and its impact on SQUID-based absolute magnetometry

T Schönau[1,2], V Zakosarenko[3], M Schmelz[1], S Anders[1], H-G Meyer[1,3] and R Stolz[1]

[1] Leibniz Institute of Photonic Technology, D-07745, Jena, Germany
[2] Friedrich-Schiller-University Jena, Institut für Festkörperphysik, Helmholtzweg 5, D-07743, Jena, Germany
[3] Supracon AG, An der Lehmgrube 11, D-07751, Jena, Germany

E-mail: thomas.schoenau@leibniz-ipht.de

Received 29 September 2017, revised 24 November 2017
Accepted for publication 28 December 2017
Published 19 January 2018

Abstract

The effect of flux trapping on the flux-voltage characteristics of multi-loop SQUID magnetometers was investigated by means of repeated cool-down cycles in a stepwise increased magnetic background field. For a SQUID with N parallel loops, N different flux offsets, each separated by Φ_0/N, were observed even in zero magnetic field. These flux offsets further split into a so called fine structure, which can be explained by minor asymmetries in the SQUID design. The observed results are discussed with particular regard to their impact on the previously presented absolute SQUID cascade vector magnetometer.

Keywords: SQUID, flux trapping, absolute vector magnetometer, SQIF, SQUID cascade

(Some figures may appear in colour only in the online journal)

1. Introduction

During several years our group has been working on the development of a low-T_c SQUID-based absolute vector magnetometer suited for mobile operation in Earth's magnetic field. This kind of sensor, denoted as SQUID cascade in previous publications [1–3], might be of great interest for airborne and ground-based geomagnetic surveys, since it outperforms conventional absolute magnetometers like optically pumped magnetometers (OPM) [4–8] in terms of noise, bandwidth, and due to its ability to measure the magnetic vector components.

The current implementation of the SQUID cascade already showed promising results in lab-based experiments as well as in first field tests. Its application potential, however, depends on the long-term stability of the magnetometer parameters such as offset, scaling, and misalignment angles, especially after thermal cycling. One key aspect is the avoidance of trapped flux in the superconducting structures, which would otherwise affect the magnetometer offset. For many geomagnetic application scenarios it would be a great benefit if such flux trapping could be prevented during cool-down[4] in magnetically unshielded environment. As discussed in detail in section 2, the SQUID cascade consists of three SQUID magnetometers of different sensitivity, the most sensitive one realized as multi-loop SQUID [9]. The parallel-connected loops of this SQUID form closed superconducting paths of comparatively large size, which are accordingly vulnerable to flux trapping. The purpose of this work is to investigate the occurrence of flux trapping in the multi-loop SQUID, compare it with theoretical expectations and discuss its impact on the absolute measurement principle.

[4] Throughout this paper, we only discuss the effect of flux trapping during cool-down cycles, even if the term 'cool-down' is not explicitly stated.

The work is structured as follows: in section 2, the idea of the SQUID cascade and the sensor design is shortly introduced. The measurement principle used to investigate flux trapping is outlined in section 3 and first experimental results are presented. In section 4, the theoretical background is developed and compared to further experimental observations. In section 5, the consequences are discussed with regard to the absolute SQUID cascade magnetometer. Finally, all results are shortly summarized in section 6 and a conclusion is drawn.

Throughout this paper, the following conventions are used: vectors are denoted by arrows ($\vec{x}$) and tensors of dimension $\geqslant 2$ are written in bold ($\boldsymbol{x}$). Upper indices are used to indicate tensor components ($\vec{x}^k$, $\boldsymbol{x}^{kl}$), whereas lower indices are used for labeling purpose only ($\vec{x}_{\text{label}}$).

2. The SQUID cascade principle

SQUIDs are generally not considered as absolute sensors due to their Φ_0-periodic flux-voltage characteristics $V(\Phi)$, with $\Phi_0 = h/2e \approx 2.07 \times 10^{-15}\,\text{Tm}^2$ being the magnetic flux quantum. In the case of a SQUID magnetometer operated in a flux-locked loop (FLL, see [10]), this ambiguity leads to a set of possible linear $V(\text{B})$ branches, each separated by magnetic field offsets of

$$\Delta B = \Phi_0/A. \tag{1}$$

Therein, A is the effective area of the SQUID magnetometer, defined by $\Phi = B \cdot A$.

Equation (1) has two important implications: first of all, for any magnetic field satisfying the relation $|B| < B_{\text{max}}$, a SQUID can be made an absolute magnetometer by reducing its effective area to $A < \Phi_0/2B_{\text{max}}$. Here, B_{max} is the estimated maximum amplitude of the considered magnetic field. Secondly, the branch on which the FLL is currently locked can be estimated by a reference measurement, provided its resolution is better than ΔB. The SQUID cascade principle depicted in figure 1 applies these ideas to a set of parallel-oriented SQUID magnetometers with significantly different effective areas in order to obtain an absolute and sensitive magnetometer. The so called reference SQUID, exhibiting the smallest effective area, is designed to perform as a low-precision absolute magnetometer in the Earth's magnetic field. Its output, however, is sufficiently precise to pick out the correct magnetic field branch measured by a SQUID of increased effective area (and sensitivity). This principle is repeated up to the most sensitive SQUID magnetometer, which determines the overall achievable accuracy and noise of the measurement[5].

In our current implementation, the SQUID cascade consists of three SQUID magnetometers with the inverse effective areas $A_1^{-1} \approx 20\,\mu\text{T}/\Phi_0$, $A_2^{-1} \approx 250\,\text{nT}/\Phi_0$ and

[5] This idea is best illustrated in terms of flux quanta: an absolute flux of e.g. 3285.17 Φ_0 in the most sensitive SQUID is reconstructed by two contributions: the integer part of 3285 Φ_0 is obtained by the smaller SQUIDs whereas the most sensitive SQUID is only used to resolve the fractional part of 0.17 Φ_0 with high resolution.

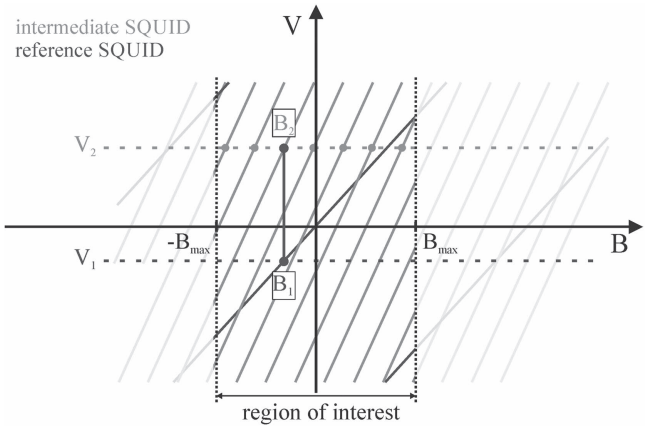

Figure 1. Principle of operation of a simplified one-axis SQUID cascade. The output of the reference magnetometer (index '1') is unique within the desired region of interest $-B_{\text{max}}$ to B_{max}. It can therefore be used to identify the correct branch of the intermediate magnetometer (index '2'). Without this additional information, the output voltage V_2 would only provide a set of possible magnetic field strengths, indicated by the light gray dots. Reproduced from [3]. © IOP Publishing. All rights reserved.

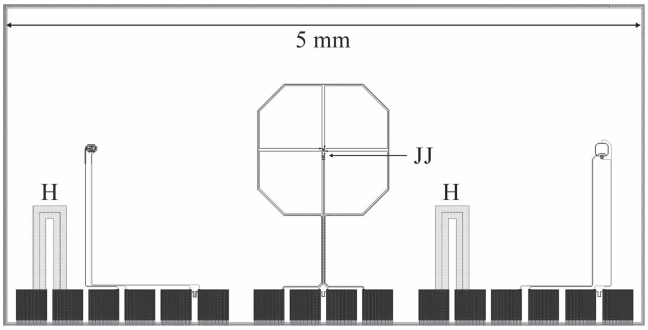

Figure 2. Design of the SQUID cascade used in this work. The reference and intermediate SQUID (left/right) are realized as single-loop SQUIDs with narrow washer. The sensitive SQUID (center) is a multi-loop SQUID with $N = 4$ loops. The position of the Josephson junctions (JJ) is indictaed by the arrow and the on-chip heating resistors are labeled as 'H'.

$A_3^{-1} \approx 9\,\text{nT}/\Phi_0$. All SQUIDs have been implemented in a sub-micron cross-type Josephson junction technology [11] which offers a significantly increased voltage swing and a reduced white noise level (about $20\,\text{fT}\,\text{Hz}^{-1/2}$ for the sensitive stage) due to the lowered junction capacitance [12]. In avoidance of relative motion and angular misalignment, all SQUIDs were realized on the same chip, as depicted in figure 2. As stated previously, the prevention of flux trapping in Earth's magnetic field $B_{\text{E}} \approx 50\,\mu\text{T}$ is crucial, so that several additional design restrictions have to be taken into account. Thus, in contrast to conventional SQUID designs, closed superconducting loops like e.g. flux transformers are not allowed. Moreover, for a long and narrow superconducting stripline of width w, the critical magnetic field for flux trapping is:

$$B_c = c \cdot \Phi_0/w^2, \tag{2}$$

with $c \approx 1$ being a constant depending on the theory taken into account [13–16]. As a consequence, the widths of all

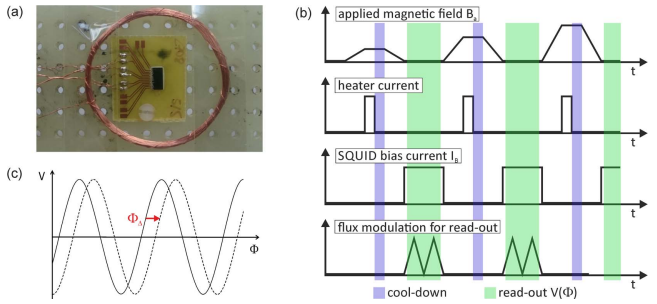

Figure 3. The flux trapping measurement was performed by immersing the chip in liquid helium using a magnetically shielded dipstick. A controllable magnetic field B_a is applied by a wire-wound copper coil (a). The detailed measurement sequence is shown in (b). If flux is trapped, the $V(\Phi)$-characteristics is shifted along the Φ-axis as depicted in (c).

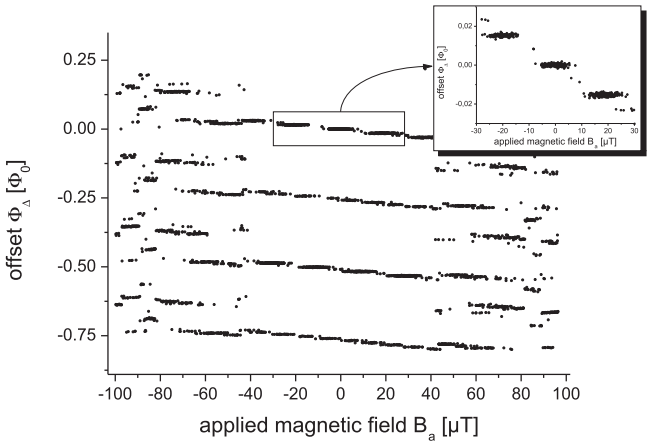

Figure 4. Result of the flux trapping measurement (3514 thermocycles) performed on the multi-loop SQUID of figure 2. For $|B_a| < 40\ \mu$T, flux is trapped in the SQUID loops only. For stronger magnetic field amplitudes, flux is also trapped in form of vortices within the superconducting striplines.

superconducting structures in our design were limited to less than 6 μm, resulting in a theoretical value of $B_c \approx 90\ \mu$T according to [16]. The real critical magnetic field, however, might be smaller due to unavoidable stripline bends and crossings, which could cause local magnetic field enhancements due to flux focusing. Furthermore, such geometries are not covered by the derivation of equation (2).

The strict application of these design restrictions bans the known methods of SQUID sensitivity enhancement, because they are either based on closed superconducting loops (e.g. multi-loop SQUID, flux transformer) or on the flux focusing effect of broad SQUID-washers. We estimated the maximum effective area of a single-loop SQUID of small washer width $w = 6\ \mu$m to be $\Phi_0/0.26\ \mu\text{T} = 7912\ \mu\text{m}^2$. Details of this calculation can be found in appendix A1. In order to compete with OPM, a compromise between consequent flux trapping prevention and sensitivity must therefore be made.

A reasonable compromise is to design the sensitive SQUID as a multi-loop magnetometer with narrow linewidths, such that flux can only be trapped within the parallel-connected superconducting loops, but not in form of vortices inside the striplines. The advantage of this approach is that the trapped flux distributes amongst the loops, thereby appearing as fractional flux quanta with opposite signs, as exemplarily depicted in figure 6(b). For a highly symmetric SQUID design, the overall magnetic moment of trapped flux is always zero, meaning that flux trapping should not be favored by the homogeneous magnetic field of the Earth.

3. Measurement method

The measurement method is illustrated in figure 3: the SQUID chip is mounted inside a magnetically shielded dipstick and immersed in liquid helium. A controllable magnetic field can be applied perpendicular to the chip by a wire-wound copper coil. It is ramped up to the value B_a, the chip is shortly heated to the normal conducting state (by applying a dc voltage to at least one of the on-chip resistors) and afterwards cooled down again. During cool-down, the SQUID bias current is set to zero in order to avoid additional magnetic fields. After a waiting time of typically 0.5–1 s, the magnetic field is ramped down and the $V(\Phi)$-characteristic of the SQUID is measured. Trapped flux causes the $V(\Phi)$-characteristics to shift horizontally, denoted as offset Φ_Δ. The detailed $\Phi_\Delta(B_a)$ dependency is obtained by an automated repetition of this procedure with stepwise increasing (or decreasing) magnetic field amplitude B_a.

The obtained measurement results might be affected by several systematic errors, such as thermal electronic drifts or the magnetization of the copper coil or other components of the dipstick. For this reason, two control mechanisms were introduced: the first is to repeat the measurement without heating the chip, resulting in a $\Phi_\Delta(B_a)$ characteristic that encompasses all environmental magnetization effects not related to trapped flux. The second is to pass the $\Phi_\Delta(B_a)$ characteristics multiple times in opposite directions (increasing versus decreasing B_a), revealing potential hysteresis effects as well as electronic drifts. By this means, the measurement setup could be tested and improved such that parasitic effects can be considered as negligible. The heating power required for the transition to the normal conducting state and the waiting time for a complete cool-down were also determined in preliminary experiments. The former was identified by successively increasing the heating voltage V_H and measuring the corresponding $\Phi_\Delta(B_a)$ characteristics until the influence of any further increase vanishes. Similarly, the waiting time for cool-down was estimated by observing the recuperation of the SQUID's $V(\Phi)$-characteristic over time.

The typical $\Phi_\Delta(B_a)$ characteristic measured for a multi-loop SQUID with $N = 4$ loops is depicted in figure 4. For an amplitude of $|B_a| < 40\ \mu$T, the offset Φ_Δ splits into four discrete levels, separated by an integer multiple of $\Phi_0/4$. A further magnetic field dependent splitting into the so called fine structure can also be observed, as shown in the inset. At about $\pm 40\ \mu$T, the $\Phi_\Delta(B_a)$ characteristics instantly change their appearance by introducing new branches and getting more 'chaotic'. We interpret this as the critical magnetic field

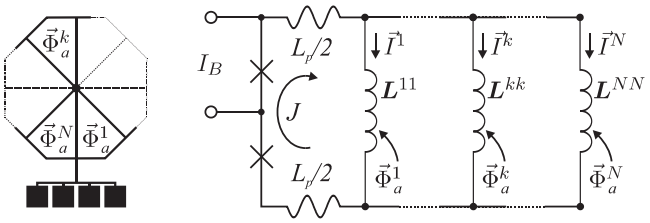

Figure 5. Equivalent cirquit diagram of a multi-loop SQUID of N loops. For $k = l$, the inductance matrix element $\boldsymbol{L}^{kl}$ describes the self-inductance of loop k, otherwise the inductive coupling between loops k and l. The SQUID's circulating current and the parasitic inductance of the Josephson junction connection lines are denoted as J and L_p, respectively.

B_c for flux trapping within the superconducting striplines of the sensor, as predicted by equation (2).

Due to the observed ambiguity of Φ_Δ even for $B_a = 0$, the state without trapped flux, defined by $\Phi_\Delta = 0$, is not obvious. $\Phi_\Delta = 0$ is therefore defined as the flux offset in the SQUID's $V(\Phi)$-characteristic that appears most frequently for $B_a = 0$. This definition will be motivated in the next chapter.

4. Theory

The theoretical background is derived by using the equivalent circuit diagram of the multi-loop SQUID depicted in figure 5. For the general case of N parallel-connected loops, the following system of equations applies during cool-down ($\boldsymbol{L} \in \mathbb{R}^{N\times N}$, $\boldsymbol{n} \in \mathbb{Z}^{N\times N}$):

$$\forall\, k\colon \vec{\Phi}_t^k = \vec{\Phi}_a^k + \sum_l \boldsymbol{L}^{kl}\vec{I}^l + L_p \cdot J, \tag{3}$$

$$\vec{\Phi}_t^k - \vec{\Phi}_t^l = \boldsymbol{n}^{kl} \cdot \Phi_0, \tag{4}$$

$$\forall\, k\colon \sum_l \vec{I}^l = J = \pm I_c \cdot \sin\left(\pi \cdot \vec{\Phi}_t^k / \Phi_0\right). \tag{5}$$

Due to the multi-loop configuration, the SQUID's magnetic flux depends on which loop is taken into account. All magnetic fluxes are therefore defined as vectors where the kth component relates to the kth loop[6]. The total magnetic flux is denoted as $\vec{\Phi}_t$ and is composed of the applied flux $\vec{\Phi}_a$, the flux caused by the supercurrents $\vec{I}$ flowing through the inductance network $\boldsymbol{L}$ (see figure 5) and a parasitic contribution proportional to the SQUID's circular current J. The latter modulates with the total flux, according to equation (5), with I_c being the critical current of a single Josephson junction. In equation (4), $\boldsymbol{n}^{kl}$ defines the amount of flux quanta trapped in the loop-pair 'kl'. In order to facilitate the above equations, we set $J = 0$ hereinafter, leading to the following equations:

$$\vec{\Phi}_t = \vec{\Phi}_a + \boldsymbol{L}\vec{I}, \tag{6}$$

$$\vec{\Phi}_t^k - \vec{\Phi}_t^l = \boldsymbol{n}^{kl} \cdot \Phi_0, \tag{7}$$

[6] The indices are defined cyclical, meaning that $k = 1 \pm N$ is equal to $k = 1$, and so on.

$$\sum_l \vec{I}^l = 0. \tag{8}$$

Since J just adds a periodically modulating magnetic flux of order $\approx\Phi_0$ to the SQUID, the proposed approximation closely oscillates around the original equations. Especially for the two cases discussed in this paper, namely $\vec{\Phi}_a = 0$ as well as the sweeping of $\vec{\Phi}_a$ to large amplitudes $>1000\ \Phi_0$, this approximation is reasonable. This is because $\vec{\Phi}_a = 0$ directly leads to $J = 0$, and for the sweeping case, all effects related to the oscillation of J should average out.

In the following, the case of a symmetric SQUID with nearest neighbor coupling between the loops is discussed, meaning $\forall\, k, \forall\, l$: $\boldsymbol{L}^{kl} = \{L$ if $k = l$, M if $|k - l| = 1$, 0 otherwise$\}$. The simplest approach is to solve this system of equations for several special cases and to obtain the general solution by superposing the obtained results.

At first, we address the case without trapped flux, i.e. $\forall\, k, \forall\, l$: $\boldsymbol{n}^{kl} = 0$, resulting in:

$$\forall\, k\colon \vec{\Phi}_t^k = \frac{1}{N}\sum_{l=1}^{N} \vec{\Phi}_a^l. \tag{9}$$

Thus, the flux distributes equally in all loops, even if it is unevenly applied. This result is ensured by the supercurrents $\vec{I}$, which balance out possible differences in the components of $\vec{\Phi}_a$.

Flux trapping is now addressed by solving the system of equations (6)–(8) for the case of a single flux quantum being trapped in loop m without any magnetic flux applied, e.g. $\vec{\Phi}_a = 0$ and $\forall\, k, \forall\, l$: $\boldsymbol{n}^{kl} = \{1$ if $m = k \neq l$, -1 if $m = l \neq k$, 0 otherwise$\}$. This fundamental excitation, further denoted as $\vec{F}_m$, causes the following flux distribution in the loops:

$$\vec{\mathrm{F}}_m^k = \begin{cases} \Phi_0 \cdot (N-1)/N, & \text{if } k = m \\ -\Phi_0/N, & \text{if } k \neq m \end{cases} \tag{10}$$

which already explains the $\Phi_0/4$—splitting observed for the four-loop SQUID in figure 4. It should be emphasized that this splitting is independent from the nearest neighbor coupling M. If, on the other hand, any coupling between the loops is neglected *a priori*, the same result can also be obtained by very simple and illustrative arguments, as explained in figure 6.

For any given flux constellation $\vec{\Phi}_t$ in the SQUID, the loop current distribution $\vec{I}$ and magnetic field energy E can be calculated by:

$$\vec{I} = \boldsymbol{L}^{-1}(\vec{\Phi}_t - \vec{\Phi}_a), \tag{11}$$

and

$$E = \frac{1}{2}\vec{I} \cdot (\vec{\Phi}_t - \vec{\Phi}_a). \tag{12}$$

Some illustrative examples of superposed fundamental excitations and their corresponding energy can be found in table 1. Apparently, the magnetic field energy is generally decreased by the nearest neighbor coupling $M < 0$, but for several symmetric flux configurations, this effect cancels out.

According to figure 4, different Φ_Δ-levels can be excited for the same value of the applied magnetic field, indicating

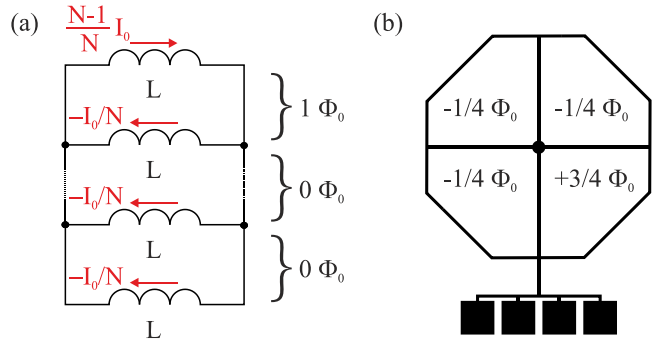

Figure 6. For a symmetric SQUID without inductive coupling between the loops, the flux distribution of a fundamental excitation can easily be derived. Let $I_0 = \Phi_0/L$, then a current of $(N-1)\cdot I_0/N$ in the excited loop will equally distribute amongst the remaining $N-1$ loops, resulting in opposite flowing currents of $-I_0/N$. The corresponding fluxes of $(N-1)\cdot\Phi_0/N$ or $-\Phi_0/N$ add up to 1 Φ_0 or 0 Φ_0 for each closed superconducting path. In (b), this flux distribution is illustrated for $N = 4$ loops.

Table 1. Several examples of superposed fundamental excitations, calculated for the case of a symmetric four-loop SQUID with nearest neighbor coupling M and zero applied flux.

Superposition	$\vec{\Phi}_t/\Phi_0$	Energy $\cdot\, 2L/\Phi_0^2$
$\vec{F}_m$, $m \in \{1,\ldots,4\}$	$\left(+\frac{3}{4}, -\frac{1}{4}, -\frac{1}{4}, -\frac{1}{4}\right)$	$\frac{3-4M/L}{4(1-2M/L)}$
	$\vdots$	
	$\left(-\frac{1}{4}, -\frac{1}{4}, -\frac{1}{4}, +\frac{3}{4}\right)$	
$\vec{F}_1+\vec{F}_2$ or $-\vec{F}_3-\vec{F}_4$	$\left(+\frac{1}{2}, +\frac{1}{2}, -\frac{1}{2}, -\frac{1}{2}\right)$	1
$\vec{F}_1+\vec{F}_3$ or $-\vec{F}_2-\vec{F}_4$	$\left(+\frac{1}{2}, -\frac{1}{2}, +\frac{1}{2}, -\frac{1}{2}\right)$	$\frac{1}{1-2M/L}$
$n\cdot\vec{F}_1$	$n\cdot\left(+\frac{3}{4}, -\frac{1}{4}, -\frac{1}{4}, -\frac{1}{4}\right)$	$n^2\cdot\frac{3-4M/L}{4(1-2M/L)}$
$\vec{F}_1-\vec{F}_2+\vec{F}_4$	$\left(+\frac{3}{4}, -\frac{5}{4}, -\frac{1}{4}, +\frac{3}{4}\right)$	$\frac{11-20M/L}{4(1-2M/L)}$
$\vec{F}_1+\vec{F}_2+\vec{F}_3+\vec{F}_4$	(0, 0, 0, 0)	0

that the flux trapping process is subject to a statistical distribution. In order to examine this effect more precisely, the dipstick measurements were repeated after the copper coil was removed. This allows for a more reproducible cool-down, since the applied magnetic field remains unchanged at almost zero and potential parasitic effects related to the coil, such as injected high frequency interferences, are eliminated as well. The results are depicted in figure 7, revealing a significant excitation probability for all four Φ_Δ-levels. Hereafter, we will compare the experimental results of figures 4 and 7 with the theoretically expected probabilities of thermal excitation.

In thermal equilibrium, the excitation probabilities of two different states α and β are expected to obey the Boltzmann distribution:

$$\frac{P_\alpha}{P_\beta} = \frac{D_\alpha}{D_\beta}\exp\left(\frac{E_\beta - E_\alpha}{k_B\cdot T}\right). \tag{13}$$

Here, P_α is the excitation probability, D_α is the degeneracy (or phase space volume) related to the energy level E_α and

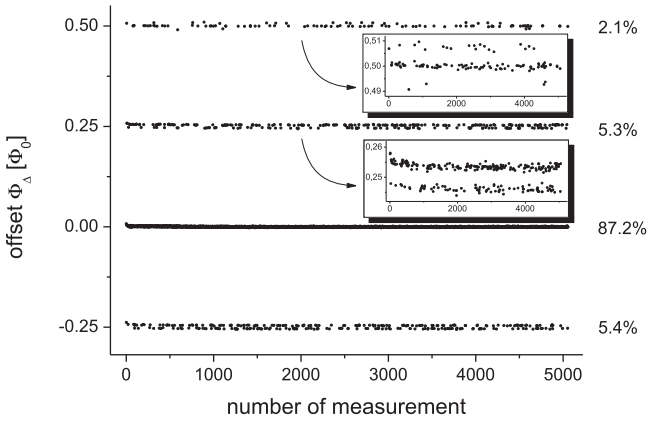

Figure 7. Flux trapping probabilities measured in magnetically shielded environment. The insets show the fine structure splittings in more detail.

$k_B \approx 1.38\times10^{-23}\,\mathrm{J\,K^{-1}}$ is the Boltzmann constant (index β analogously). Since flux trapping usually occurs very close to the transition temperature T_c of the superconductor [17], $T \approx 9.2\,\mathrm{K}$ is a reasonable value for the niobium based SQUIDs used in this work.

According to equations (12) and (13), the most probable configuration for trapped flux is $\vec{\Phi}_t \approx \vec{\Phi}_a$, meaning that the flux distribution in the loops tries to 'match' the spatial distribution of the applied magnetic field. Configurations like $\left(+\frac{1}{2}, +\frac{1}{2}, -\frac{1}{2}, -\frac{1}{2}\right)\Phi_0$ will therefore be favored by magnetic field gradients, whereas $\left(+\frac{1}{2}, -\frac{1}{2}, +\frac{1}{2}, -\frac{1}{2}\right)\Phi_0$ is most probable if an appropriate magnetic quadrupole moment is applied. Homogeneous magnetic fields, on the contrary, do not favor flux trapping in the loops, providing the SQUID is perfectly symmetric. Thus, when cooled down in Earth's magnetic field, the state without any trapped flux should be the most probable. In our field-cooling experiments, however, the magnetic field was applied by the small wire-wound copper coil depicted in figure 3(a). Since its homogeneity is estimated to be relatively poor, the excitation probabilities of the four Φ_Δ-levels in figure 4 modulate with the applied magnetic field, or more specifically, with the applied parasitic gradient.

In case of zero-field cooling, the excitation probabilities were calculated to be 97.93% for $\Phi_\Delta = 0$, 0.90% for $\Phi_\Delta = \pm\Phi_0/4$ and 0.27% for $\Phi_\Delta = \pm\Phi_0/2$. Details of this calculation can be found in appendix A2. The excitations measured in figure 7 tend to be distributed more evenly than predicted, which might be caused by the fast (non-equilibrium) cool-down procedure. Small residual gradients or the used approximation $J = 0$ might affect these results as well. The theoretical values, however, demonstrate that flux trapping in the SQUID loops may appear with significant probability even in zero magnetic field.

The remaining task is to determine the cause of the observed fine structure. Principally, such splitting could be explained by asymmetries[7] in $\boldsymbol{L}$. For example, a flux quantum trapped in a simple two-loop SQUID with loop inductances

[7] $\boldsymbol{L}$ is denoted symmetric if it is invariant under cyclic permutation of the loops: $\boldsymbol{L}^{kl} = \boldsymbol{L}^{k+j,l+j}$, with $k, l, j \in \mathbb{Z}$.

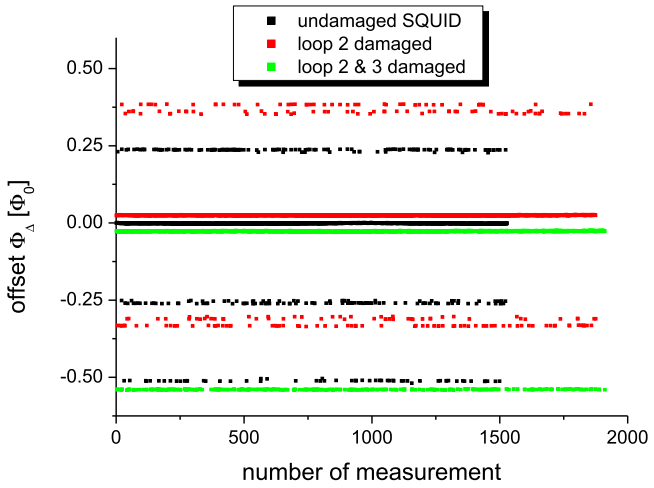

Figure 8. Distribution of Φ_Δ for an (un)damaged four-loop SQUID. In the undamaged case, four levels with a fine structure splitting of 8 mΦ_0 are visible. After damaging loop '2', only three levels appear and the fine structure splits into 8 mΦ_0 and 22 mΦ_0. When loop '2' and '3' are destroyed, the SQUID is symmetric again, exhibiting two levels without any visible fine structure. For clarity, the black, red and green curves were slightly shifted relative to each other.

$\boldsymbol{L}^{11} = L_1$, $\boldsymbol{L}^{22} = L_2$ and $\boldsymbol{L}^{12} = \boldsymbol{L}^{21} = 0$ contributes $\pm\Phi_0 L_1/(L_1 + L_2)$ and $\mp\Phi_0 L_2/(L_1 + L_2)$ to the two loops. The associated flux offset will therefore differ from $\pm\Phi_0/2$ if $L_1 \neq L_2$. The fundamental disadvantage of such an asymmetry is that flux trapping would also be favored by homogenous magnetic fields, meaning that in a later application scenario, Φ_Δ would depend on the SQUID's orientation relative to Earth's magnetic field during cool-down. Since Φ_Δ slightly mismatches the levels $\pm n \cdot \Phi_0/N$, this dependency appears as a quasi-continuously drift $\Phi_\Delta(B_a)$, similar to the one shown in figure 4. It is therefore important to study the origin of the observed fine structure in more detail, especially whether it is caused by an asymmetric inductance matrix $\boldsymbol{L}$.

To answer this question, the same four-loop SQUID was measured in three different conditions: Starting with the undamaged SQUID, loops '2' and '3' were interrupted by a diamond file one after another and for each intermediate state, the flux offset distribution Φ_Δ was measured in zero applied magnetic field. The results, shown in figure 8, are interpreted the following way: After damaging loop '2', a three-loop SQUID with an additional major asymmetry is obtained. This is because the inductive coupling between loops '1' and '3' is now much weaker than the coupling between other adjacent loops. Once loop '3' is destroyed too, the SQUID seems to be perfectly symmetric since there is no observable fine structure splitting.

A significant asymmetry in the inductance matrix $\boldsymbol{L}$ of the undamaged SQUID, for example due to fabrication inaccuracies, is therefore very unlikely. Instead, the fine structure is expected to originate in the asymmetric placement of the Josephson junctions between loops '1' and '4'. This close proximity causes non-negligible inductive couplings $\boldsymbol{L}^{11} \leftrightarrow L_p$ and $\boldsymbol{L}^{44} \leftrightarrow L_p$ between the adjacent SQUID loops and the parasitic inductance of the junction connection lines. As a result, there is an additional parasitic flux Φ_p seen by the SQUID, which can be described by the simple model:

$$\Phi_p \propto \vec{\Phi}_t^{\,1} + \vec{\Phi}_t^{\,4}. \tag{14}$$

There are several arguments supporting this theory. First of all, it explains the disappearance of the fine structure if the loops '2' and '3' are interrupted. Moreover, the two-fold fine structure splitting for $\Phi_\Delta = \pm\Phi_0/4$ as well as the three-fold splitting of $\Phi_\Delta = \pm\Phi_0/2$, both observed in figure 7, follow directly from applying equation (14) to the cyclic permutations of $\left(+\frac{3}{4}, -\frac{1}{4}, -\frac{1}{4}, -\frac{1}{4}\right)\Phi_0$ and $\left(+\frac{1}{2}, +\frac{1}{2}, -\frac{1}{2}, -\frac{1}{2}\right)\Phi_0$, respectively.

In theory, the presence of L_p also affects the inductive couplings $\boldsymbol{L}^{14}$ and $\boldsymbol{L}^{41}$ by the indirect linkage $\boldsymbol{L}^{11} \leftrightarrow L_p \leftrightarrow \boldsymbol{L}^{44}$. This, however, is a higher order effect that we expect to be negligible. We therefore consider the inductance matrix $\boldsymbol{L}$ as highly symmetric and conclude that flux trapping in the loops should not significantly be favored in the Earth's homogenous magnetic field.

5. Impact on absolute magnetometry

The experimental and theoretical findings are now discussed with regard to their impact on the SQUID cascade principle. First of all, it should be emphasized that flux trapping within the superconducting striplines could be avoided for $|B_a| < 40\ \mu$T by a consequent linewidth restriction. This is already about half the value needed for a save cool-down in Earth's magnetic field. We are confident that further improvements can be achieved by optimization of the SQUID design and the fabrication processes as well. Hereby, the most promising approaches are even smaller linewidths and the reduction of flux focusing effects due to large filling factors. The latter are expected to be significant in the used comb-shaped bond pad geometry, which is introduced in [2].

The essential problem of multi-loop SQUIDs is that flux can also be trapped within the loops. Since the loop inductance is usually quite large, the thermal excitation of flux quanta gets relevant even in zero magnetic fields, meaning that a change of the flux offset by integer multiples of Φ_0/N can generally not be avoided after cool-down. Due to their quantization, these offset changes can be compensated computationally, provided they are correctly identified and the fine structure splitting is negligible. We are going to discuss potential methods of identification for several scenarios, thereby assuming that flux is only trapped in the loops but not within the striplines.

5.1. Best case scenario

In the optimal case, $\boldsymbol{L}$ can be considered as symmetric and the SQUID is cooled down in a homogenous magnetic field. Since flux trapping is not favored by the applied field, the situation should be equivalent to the zero-field cool-down depicted in figure 7: all flux quanta are thermally excited with probabilities that are symmetrically distributed around the most probable

flux-free state. Furthermore, only small amounts of flux are trapped, resulting in just a few excited fine structure levels.

The different Φ_Δ-levels can be distinguished by comparing the output of the three-level cascade with the intermediate result of the second cascade level. If the multi-loop SQUID changes its offset, the mentioned difference signal is directly affected. In order to be able to directly identify the different offsets, the accuracy tolerance for the intermediate SQUID must be decreased by factor N to at least $\Phi_0/(N \cdot A_3)$, corresponding to 2.25 nT for the presented design. The best case scenario, however, allows for a second approach: by repeatedly heating the chip a few times, the probability distribution can be measured, easily revealing the flux-free state.

5.2. Realistic scenario

Minor asymmetries in $\boldsymbol{L}$ as well as gradients in the order of $\gtrsim 1\ \mu\mathrm{T\,m^{-1}}$ during cool-down may influence the excitation probabilities of the Φ_Δ-levels. The alternative approach of identifying these levels by their probability distribution is therefore inapplicable, leaving only the conventional method.

Compared to the best case scenario, more flux will be trapped in the loops, resulting in the excitation of a few more fine structure levels. Nevertheless, we estimate Earth's magnetic field in all relevant application scenarios to be more homogenous than the field applied by the small wire-wound coil used for the measurement in figure 4. The drift of the Φ_Δ-levels caused by the fine structure should therefore be less than in figure 4. It should further be noted that our current design still allows a significant reduction of the fine structure splitting, since it was not optimized for a small parasitic inductance L_p.

5.3. Worst case scenario

If the symmetry of $\boldsymbol{L}$ is worse than expected or unusual strong gradients are applied during cool-down, large amounts of flux can be trapped in the loops. In this situation, the Φ_Δ-levels are drifting strongly with the applied magnetic field (or gradient) and thus may overlap. Although a correction of the sensor offset is not possible in this case, it should be emphasized that, due to the cascade principle, the multi-loop SQUID only contributes the fractional part of a flux quantum to the measurement. Thus, offset deviations are automatically restricted to $\pm 0.5\ \Phi_0$ (corresponding to ± 4.5 nT for the presented design) even if larger amounts of flux are trapped. This holds true as long as the other sensor stages of lower sensitivity remain reproducible. We numerically estimated the magnetic stray field associated with the fundamental excitation $\vec{F}_m$: for our current design, an average magnetic field of 0.7 pT is coupled to the intermediate SQUID stage. Thus, the above statement holds true unless several thousand flux quanta are trapped in the loops of the sensitive SQUID. This, however, can be ruled out in Earth's magnetic field.

6. Summary

We experimentally investigated flux trapping during cool-down in multi-loop SQUIDs by observing the associated flux shifts in their $V(\Phi)$-characteristics. Due to the linewidth restriction $w \leqslant 6\ \mu$m used in the sensor design, flux trapping in the form of vortices within the striplines could be prevented for magnetic field amplitudes of less than $40\ \mu$T. Instead, magnetic flux was only trapped in the network of parallel-connected SQUID loops, resulting in offset shifts quantized to Φ_0/N, with N being the number of loops. Small deviations from this quantization rule, herein denoted as 'fine structure', have also been noticed and are expected to originate mainly in the asymmetry caused by the eccentric placement of the Josephson junctions between two adjacent loops.

A theoretical analysis of the flux trapping process was developed which confirms all experimental observations. In particular it could be shown that flux trapping in the loops occurs due to thermal excitation and that the excitation probabilities are non-negligible even in magnetically shielded environment. This result can be considered as a drawback for the absolute magnetometer concept presented in this work, because each thermocycle may result in an alteration of the magnetometer offset. On the other hand, it should be possible to identify and computationally correct these quantized offset changes in typical application scenarios.

It should further be underlined that even if these corrections are not applied, the offset deviations are restricted to $\pm 0.5\ \Phi_0$, corresponding to only a few nanoteslas. This is a significant improvement compared to previous publications in which SQIFs were proposed as absolute magnetometers, suffering from offset variations of a few microteslas if cooled down in the Earth's magnetic field [18, 19].

Appendix

A1. Maximum effective area

The inductance of a SQUID with a narrow square pickup loop is [20]:

$$L_{SQ} = 2\mu_0/\pi \cdot (d + w) \cdot [\ln(1 + d/w) + 0.5], \qquad (15)$$

with μ_0 the vacuum permeability, d the inner diameter and w the width of the washer. We are searching for the maximum value of d, such that the inductance parameter:

$$\beta_L = 2I_0 \cdot L_{SQ}/\Phi_0 \qquad (16)$$

does not exceed its optimum value $\beta_L \approx 1$ [21]. Assuming a critical junction current of $I_0 = 5\ \mu$A and $w = 6\ \mu$m, the inner diameter is restricted to $d \lesssim 86\ \mu$m, resulting in an effective area [20]:

$$A = d \cdot (d + w) \qquad (17)$$

limited to $A = 7912\ \mu\mathrm{m}^2$ or $A^{-1} = 260\ \mathrm{nT}/\Phi_0$.

A2. Excitation probabilities

The excitation probabilities of the four Φ_Δ-levels are calculated according to equation (13) for the case of zero applied magnetic field ($\vec{\Phi}_a = 0$). The loop inductance and the nearest neighbor coupling between the loops were estimated numerically in FastHenry [22], resulting in $L = 1.94$ nH and

$M = -0.26$ nH. The problem of calculating the excitation probability for a particular Φ_Δ-level is, that, due to the underlying Φ_0-periodicity, each level corresponds to an infinite number of possible flux configurations. For example, the level $\Phi_\Delta = -1/4\,\Phi_0$ corresponds to all permutations of $\left(+\frac{3}{4}, -\frac{1}{4}, -\frac{1}{4}, -\frac{1}{4}\right)\Phi_0$ or $\left(+\frac{3}{4}, -\frac{5}{4}, -\frac{1}{4}, +\frac{3}{4}\right)\Phi_0$ as well as to all their $(4n + 1)$-multiples, with $n \in \mathbb{Z}$. But due to their much larger energy, the higher order states can usually be neglected.

A reasonable approximation for the levels $\Phi_\Delta = \pm 1/4\,\Phi_0$ is therefore to calculate the excitation probability of all permutations of $\left(+\frac{3}{4}, -\frac{1}{4}, -\frac{1}{4}, -\frac{1}{4}\right)\Phi_0$. Using the energy given in table 1 and a degeneracy of four different permutations, the result is:

$$\frac{P\left(\Phi_\Delta = \pm\frac{\Phi_0}{4}\right)}{P(\Phi_\Delta = 0)} = 0.92\%.$$

For comparison purposes it should be mentioned that the neglected permutations of $\left(+\frac{3}{4}, -\frac{5}{4}, -\frac{1}{4}, +\frac{3}{4}\right)\Phi_0$ would have contributed with only 5.2×10^{-10}.

The level $\Phi_\Delta = \pm 1/2\,\Phi_0$ is approximated by the four cyclic permutations of $\left(+\frac{1}{2}, +\frac{1}{2}, -\frac{1}{2}, -\frac{1}{2}\right)\Phi_0$ and two cyclic permutations of $\left(+\frac{1}{2}, -\frac{1}{2}, +\frac{1}{2}, -\frac{1}{2}\right)\Phi_0$ (see table 1 for energy formulas), resulting in:

$$\frac{P(\Phi_\Delta = \pm\Phi_0/2)}{P(\Phi_\Delta = 0)} = 0.28\%.$$

Thus, the probabilities are:

$$P(\Phi_\Delta = 0) = 97.93\%,$$
$$P(\Phi_\Delta = +\Phi_0/4) = 0.90\%,$$
$$P(\Phi_\Delta = -\Phi_0/4) = 0.90\%,$$
$$P(\Phi_\Delta = \pm\Phi_0/2) = 0.27\%.$$

For all calculations, a temperature of $T = 9.2$ K was chosen.

ORCID iDs

T Schönau https://orcid.org/0000-0003-1533-7434

References

[1] Schönau T, Schmelz M, Zakosarenko V, Stolz R, Meyer M, Anders S, Fritzsch L and Meyer H-G 2013 SQUID-based setup for the absolute measurement of the Earth's magnetic field *Supercond. Sci. Technol.* **26** 35013

[2] Schönau T, Zakosarenko V, Schmelz M, Stolz R, Anders S, Linzen S, Meyer M and Meyer H-G 2015 A three-axis SQUID-based absolute vector magnetometer *Rev. Sci. Instrum.* **86** 105002

[3] Schönau T, Zakosarenko V, Schmelz M, Stolz R, Anders S, Linzen S, Meyer M, Faßbinder J W E and Meyer H-G 2017 Absolute calibration of a three-axis SQUID-cascade vector magnetometer *Meas. Sci. Technol.* **28** 15107

[4] Budker D and Romalis M 2007 Optical magnetometry *Nat. Phys.* **3** 227–34

[5] Budker D and Kimball D F J 2013 *Optical Magnetometry* ed D Budker and D F J Kimball (Cambridge: Cambridge University Press)

[6] Scholtes T, Schultze V, IJsselsteijn R, Woetzel S and Meyer H-G 2011 Light-narrowed optically pumped M_x magnetometer with a miniaturized Cs cell *Phys. Rev.* A **84** 43416

[7] Anon Scintrex CS-3 Cesium magnetometer datasheet http://scintrexltd.com/wp-content/uploads/2017/03/ CS-3-Brochure-762711_3.pdf

[8] Anon 2013 Geometrics G-822A airborne cesium magnetometer ftp://geom.geometrics.com/pub/mag/DataSheets/G822ADS.pdf

[9] Drung D, Knappe S and Koch H 1995 Theory for the multiloop dc superconducting quantum interference device magnetometer and experimental verification *J. Appl. Phys.* **77** 4088

[10] Drung D 1996 Advanced SQUID read-out electronics *SQUID Sensors: Fundamentals, Fabrication and Applications* ed H Weinstock (Dordrecht: Springer) pp 63–117

[11] Anders S, Schmelz M, Fritzsch L, Stolz R, Zakosarenko V, Schönau T and Meyer H-G 2009 Sub-micrometer-sized, cross-type Nb–AlO_x–Nb tunnel junctions with low parasitic capacitance *Supercond. Sci. Technol.* **22** 64012

[12] Schmelz M, Stolz R, Zakosarenko V, Anders S, Fritzsch L, Schubert M and Meyer H-G 2011 SQUIDs based on submicrometer-sized Josephson tunnel junctions fabricated in a cross-type technology *Supercond. Sci. Technol.* **24** 15005

[13] Likharev K K 1971 The formation of a mixed state in planar semiconductor films *Radiophys. Quantum Electron.* **14** 722–7

[14] Maksimova G M 1998 Mixed state and critical current in narrow semiconducting films *Phys. Solid State* **40** 1607–10

[15] Clem J R 1998 Vortex exclusion from superconducting strips and SQUIDs in weak perpendicular ambient magnetic fields *APS March Meeting Abstracts*

[16] Kuit K, Kirtley J, van der Veur W, Molenaar C, Roesthuis F, Troeman A, Clem J, Hilgenkamp H, Rogalla H and Flokstra J 2008 Vortex trapping and expulsion in thin-film YBCO strips *Phys. Rev.* B **77** 134504

[17] Stan G, Field S B and Martinis J M 2004 Critical field for complete vortex expulsion from narrow superconducting strips *Phys. Rev. Lett.* **92** 97003–4

[18] Caputo P, Oppenländer J, Häussler C, Tomes J, Friesch A, Träuble T and Schopohl N 2004 High-performance magnetic field sensor based on superconducting quantum interference filters *Appl. Phys. Lett.* **85** 1389

[19] Caputo P, Tomes J, Oppenlander J, Haussler C, Friesch A, Trauble T and Schopohl N 2005 Superconducting quantum interference filters as absolute magnetic field sensors *IEEE Trans. Appl. Supercond.* **15** 1044–7

[20] Cantor R and Koelle D 2004 Practical DC SQUIDS: configuration and performance *The SQUID Handbook: Fundamentals and Technology of SQUIDs and SQUID Systems* ed J Clarke and A I Braginski vol I (Weinheim: Wiley) pp 171–217

[21] Tesche C D and Clarke J 1977 dc SQUID: noise and optimization *J. Low Temp. Phys.* **29** 301–31

[22] Kamon M, Tsuk M J and White J K 1994 FASTHENRY: a multipole-accelerated 3-D inductance extraction program *IEEE Trans. Microw. Theory Tech.* **42** 1750–8